

ARTICLE

Open Access

Tuning the light emission of a Si micropillar quantum dot light-emitting device array with the strain coupling effect

Yepei Mo^{1,2}, Xiaolong Feng³, Li Zhang^{1,2}, Renhou Han^{2,4}, Rongrong Bao^{1,2,5} and Caofeng Pan^{2,4,5}

Abstract

Using an optical signal to realize sensing of a strain signal is a promising application for tactile sensors. However, most research is now focused on piezophototronic LED arrays, which are difficult to incorporate into the Si-based semiconductor industry. Due to the poor photoelectric performance of Si-based devices caused by the indirect band gap of Si, it has always been challenging to construct high density light-emitting devices with Si. Here, a Si-based quantum dot light-emitting device (QLED) array composed of p-Si micropillars is designed and fabricated, and the mechanism for modulation of the strain coupling effect in Si on the electroluminescence performance of Si-based QLEDs is studied. The introduction of QDs easily provides efficient and adjustable light emission and meets the requirements of different practical applications. The emission intensity of the QLED depends on the injected current density, and the transportation processes of the carriers can be modulated by the strain coupling effect. The combination of Si-based photonic devices with pressure sensing may have a significant impact on the fields of electronic skin and human-machine interfaces. More importantly, this technology is fully compatible with the dominant Si-based semiconductor industry. Therefore, it shows promise in realizing the integration of large-scale Si-based photonic devices and expanding their application fields.

Introduction

Research on tactile sensors has been developed for years^{1–6} and compared to electrical signals^{7–10}, optical signals are easier to obtain and analyze and also have the advantages of visualization and low crosstalk^{11,12}. Application of optical signals in tactile sensors by introducing the piezophototronics effect^{13,14} constitutes a promising strategy. Semiconductor materials with wurtzite structures, such as ZnO¹⁵, CdS¹⁶, and GaN¹⁷, have been used to map pressure distributions with piezoelectric nanowire (NW) light-emitting device (LED) arrays in the previous

studies^{18–23}. Although the piezoelectric NW LED, array shows great potential for application in producing electronic skin²⁴, human-machine interfaces and pressure sensors^{25,26}, the defects in piezoelectric materials result in many defect emissions at the traditional p-n junction, which is not conducive to acquisition and processing of the optical signals of sensor arrays^{27–32}. The excellent properties of quantum dots, such as narrow emission spectra, tunable color spectra and high stability, provide effective solutions to overcome this disadvantage³³. On the other hand, first-generation semiconductor materials, such as Si, dominate the semiconductor industry³⁴. It is still a challenge to combine pressure sensing with the Si-based electronic industry^{35,36}. Due to the centrosymmetric crystal structure of Si, it cannot produce piezoelectric polarization like noncentrosymmetric semiconductors. There is a polarization phenomenon induced by inhomogeneous strain in semiconductor materials, the flexoelectric effect, which is different from the piezoelectric

Correspondence: Rongrong Bao (baorongrong@binn.cas.cn) or Caofeng Pan (cfpan@binn.cas.cn)

¹School of Chemistry and Chemical Engineering, Guangxi University, Nanning, Guangxi 530004, P. R. China

²CAS Center for Excellence in Nanoscience, Beijing Key Laboratory of Micronano Energy and Sensor, Beijing Institute of Nanoenergy and Nanosystems, Chinese Academy of Sciences, Beijing 100083, P. R. China
Full list of author information is available at the end of the article
These authors contributed equally: Yepei Mo, Xiaolong Feng

© The Author(s) 2022



Open Access This article is licensed under a Creative Commons Attribution 4.0 International License, which permits use, sharing, adaptation, distribution and reproduction in any medium or format, as long as you give appropriate credit to the original author(s) and the source, provide a link to the Creative Commons license, and indicate if changes were made. The images or other third party material in this article are included in the article's Creative Commons license, unless indicated otherwise in a credit line to the material. If material is not included in the article's Creative Commons license and your intended use is not permitted by statutory regulation or exceeds the permitted use, you will need to obtain permission directly from the copyright holder. To view a copy of this license, visit <http://creativecommons.org/licenses/by/4.0/>.

effect and is not limited by semiconductor lattice symmetry. The application of the flexoelectric effect has drawn extensive attention from researchers^{37–42}. In particular, the strain modulation mechanism of Si has attracted considerable interest. However, since the theoretical flexoelectric coefficient of Si is only $\sim 1 \text{ nC m}^{-1}$, the flexoelectric effect in Si has not attracted much attention⁴³. Due to the influence of practical factors, the reported experimental flexoelectric coefficients of Si⁴² are as high as $\sim 78 \text{ nC m}^{-1}$. Recently, flexoelectronic effects in centrosymmetric semiconductors such as Si have been reported; the flexoelectric polarization field has a significant impact on the Schottky barrier at the metal-semiconductor interface and the distribution of free carriers inside the semiconductor, and it, therefore, tunes the process for transport of charges⁴². The flexoelectronic effect provides a promising strategy for expanding the applications of Si in pressure sensing.

Here, we report an ordered Si-based quantum dot light-emitting device (QLED) array. The flexoelectric polarization field of Si induced by the strain gradient has a significant effect on the local carrier concentration distribution, thereby realizing regulation of the carrier transport characteristics. As a result, external strain can be used to modulate the electroluminescence performance of the Si-based QLED array effectively over a wide range. In particular, the electroluminescence density of the Si-based QLED array is increased by $\sim 600\%$ under pressure of $\sim 13.8 \text{ GPa}$. This technology shows promise for the application of Si-based devices for pressure distribution mapping through optical signals, and it may contribute to research in the Si-based semiconductor industry on human-machine interfaces, electronic skin, and tactile sensing. Moreover, complete compatibility with the Si-based electronic industry makes possible the realization and large-scale integration of high-performance Si-based photonic devices.

Materials and methods

Fabrication process for Si micropillars

First, p-Si was cleaned with acetone and ethanol, and then a wafer was immersed in HF (1%) for 2 min to remove organics remaining on the Si surface. Then, the Si wafer was treated with O_2 -plasma for 10 min, the photoresist (SUN 9i 50 cP, Suntific Materials, Ltd.) was spin-coated onto the surface of the Si wafer at a speed of 4000 rpm for 60 s, and the patterned photoresist mask was formed by exposure to ultraviolet light. Finally, p-Si with ordered micropillars on the surface was obtained by ICP (SI 500, SENTECH). In the etching process of the Si wafer, SF_6 , O_2 and Ar gases were applied to the vacuum chamber with flow rates of 30, 6, and 10 sccm, respectively. After etching, the Si wafer with micropillars was soaked in acetone to remove the remaining photoresist.

Fabrication process for Si-based QLED arrays

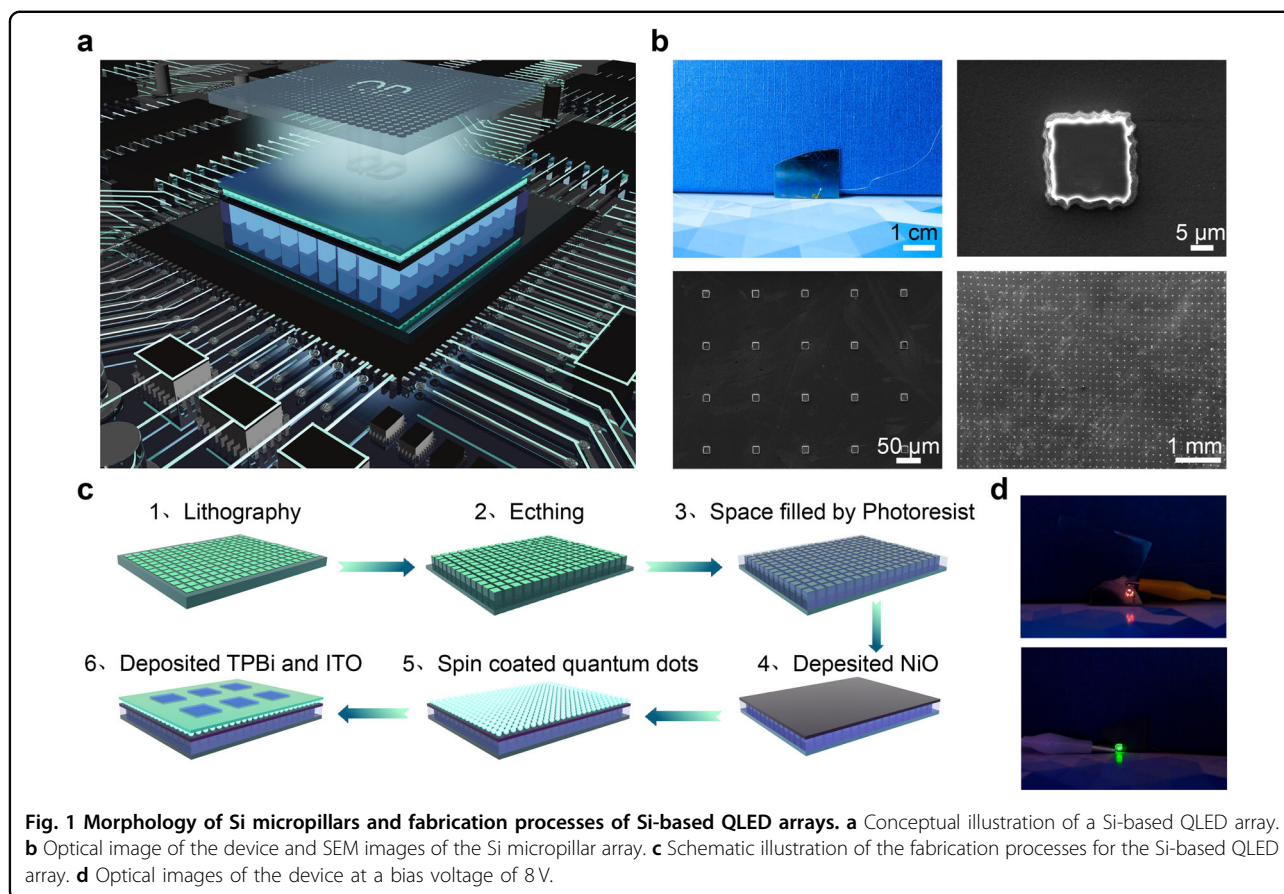
The entire surface of the Si wafer was covered with photoresist (SU8 1040, Gersteltec Sàrl) and then etched by RIE (2000CE, South Bay Technology, Inc.) to expose the tips of the micropillars. A layer of NiO was deposited on the surface of Si micropillars by magnetron sputtering (PVD75, Kurt J. Lesker) at 100 W for 30 min (200 nm). Then, the CdSe/ZnS quantum dots (QDs, in n-hexane, 15 mg mL^{-1}) were spin-coated onto the surface of the NiO layer at 2000 r.p.m. for 40 s and annealed at 60°C for 5 min. Subsequently, a 1,3,5-tris(2-*N*-phenylbenzimidazolyl)benzene (TPBi) layer (800 nm) was deposited via thermal evaporation as an electron transport layer. Finally, a layer of patterned ITO (100 nm) serving as the top electrode was deposited on the TPBi layer by magnetron sputtering, and a layer of Ag (50 nm) serving as the bottom electrode was deposited on the back of the Si wafer by magnetron sputtering.

Characterization and measurement of the Si-based QLED array

The Si micropillars and Si-based QLED array were characterized by field-emission scanning electron microscopy (SU8020, Hitachi, Ltd). The Si-based QLED array device was powered by a Maynuo DC Source Meter M8812, and the EL spectra of the device were obtained with an Ocean Optics Spectrometer (QE65000). The I - V and I - t curves of the device were measured with a semiconductor test system (1500, Keithley). An optical image of the device emitting performance was taken with a Zeiss Observer Z1 camera.

Results and discussion

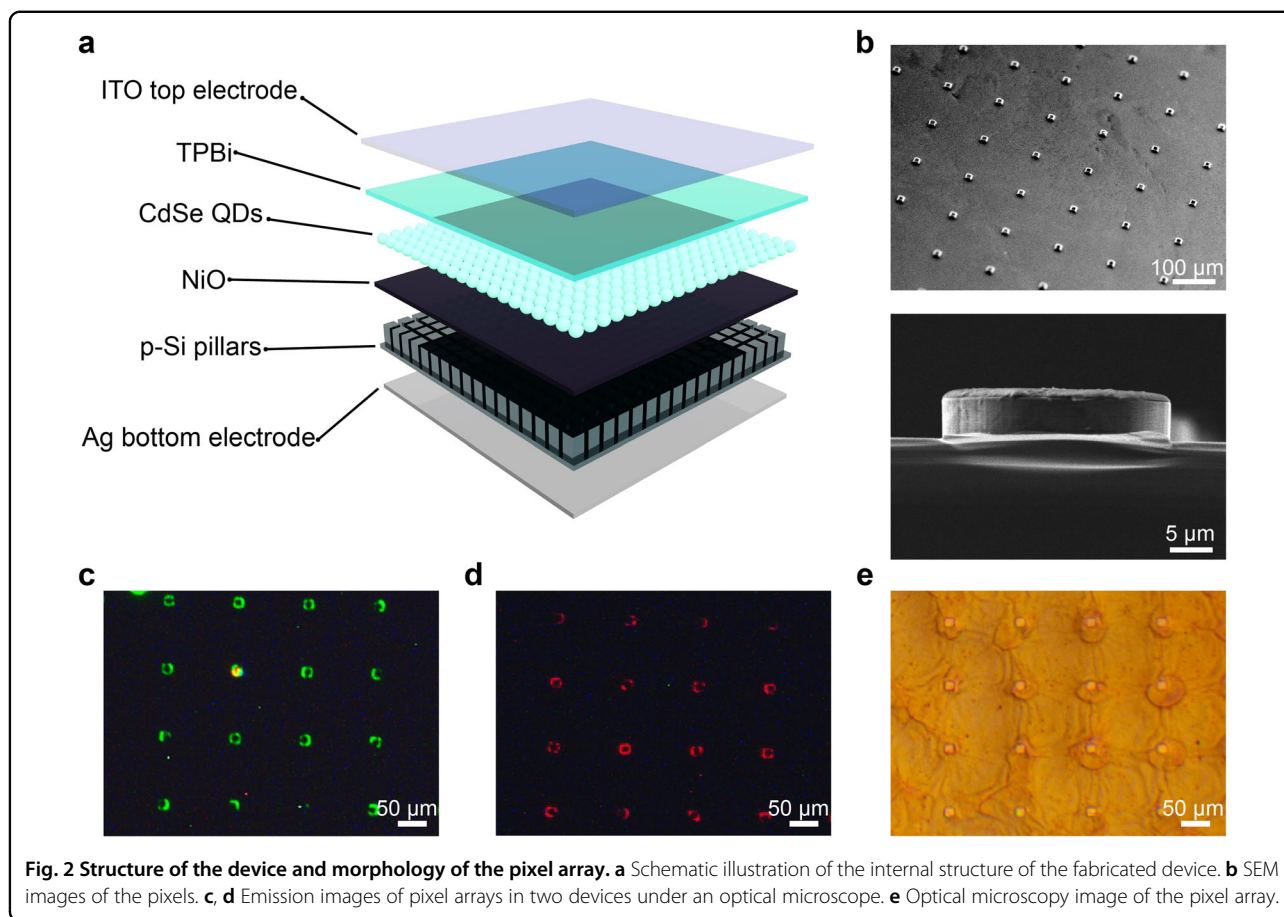
Micropillars were etched the Si wafer so that the structure can concentrate stress and produce greater pressure. On the other hand, the Si micropillars were used directly as a hole transport layer to fabricate the QLED and form the pixel points for pressure sensing. The concept of the Si-based QLED array is illustrated in Fig. 1a. The fabrication process of the Si-based QLED array is shown in Fig. 1c. The cleaned p-type Si wafers were spin-coated by a photoresist, and then a patterned photoresist was used as a mask. Then, a large-scale Si micropillar array was obtained through inductively coupled plasma (ICP) etching, which was also used as a hole transport layer (HTL). Subsequently, to ensure the flatness of the whole device, the space between the Si micropillars was filled with photoresist (SU8 1040), and the tips of the micropillars were exposed by reactive ion etching (RIE). The photoresist was used as an isolation layer between the micropillars. Then, a layer of p-NiO film was deposited on the surface of the Si micropillars by magnetron sputtering to serve as an electron barrier layer (EBL), and CdSe QDs were spin-coated as a light-emitting layer. After that, TPBi



was evaporated to serve as an electron transport layer (ETL). The final procedure involved depositing patterned ITO on TPBi as the transparent top electrode and Ag on the back of the Si wafer as the bottom electrode. With the same device structure, light emission of multiple wavelengths can be easily realized by using different QDs, which greatly simplifies the fabrication of the device to meet the emission wavelength requirements of different application scenarios. Figure 1b contains optical images of the Si-based QLED array and SEM images of the Si micropillars. The sides of the approximately square Si micropillars measured 20 μm , and the distance between the two micropillars was 100 μm . Figure 1d shows optical images of the red and green QLED devices operating under a bias voltage of 8 V.

The patterned Si array structure is easily obtained through design and processing. Before devices were fabricated, we characterized the electrical properties of the Si micropillars under pressure to study the influence of external loading force on the current. The luminescence characteristics of the device were completely determined by the quantum dots, and the light emission wavelength of the device can be easily adjusted by using quantum dot materials of different sizes. The structure of the designed

device is shown in Fig. 2a. After filling with photoresist for insulation, the gap between the micropillars was covered by photoresist and formed the same plane as the exposed tips of the micropillar array. Only the part in contact with the micropillars provides transmission channels for holes. Therefore, the sizes of the light-emitting pixels can be well matched with the Si micropillar array, and light emission will not be observed from the section without micropillars. Figure 2b shows the morphology of the Si micropillars. In addition, the sizes of light-emitting pixels are defined by the Si micropillar array. The red and green light emitted by the Si-based QLED pixel array under an 8 V bias voltage are shown in Fig. 2c, d. Each micropillar can be used as a pixel and a single QLED. Light emission from the array was uniform, and there was no crosstalk between adjacent light-emitting pixels, which is important for applications of sensor arrays. An optical microscopy image of pixels without bias voltage is shown in Fig. 2e. After the Si-based QLED array device was fabricated, electroluminescence (EL) spectra of the devices were obtained. As shown in Fig. 3b, d, the EL intensities of the red and green QLED devices gradually increased with increasing bias voltage, and the EL peak positions of the red (633 nm) and green (530 nm) QLEDs remained



unchanged with increasing bias voltage. Figure 3a, c clearly shows that the EL emission peak positions of the red and green devices corresponded to the photoluminescence (PL) emission peak positions of CdSe quantum dots. This indicates that luminescence from the fabricated device comes only from the quantum dots and exhibits narrow full widths at half-maxima (FWHM) of 24 and 33 nm for green and red QLED devices, respectively. Notably, the size and positions of the Si micropillar array exhibited good uniformity and high precision due to control of the lithographic processing parameters. The I - V curve and corresponding energy level diagram of the Si-based QLED array are shown in Fig. 3e, f, respectively.

The measurement system composed of a semiconductor test system, dynamometer and three-dimensional stages for electrical property characterization is shown in Fig. 4a. The three-dimensional stages and dynamometer were used to apply pressure to the Si micropillar array because only a small area of the Si micropillar array was under pressure, so a large pressure was generated on the Si surface from the bottom. When the dynamometer applied a 20 N force on top of the micropillars, a pressure of approximately 5.6 GPa was generated on the Si surface below the micropillars; this

pressure began to deform the lattice of the Si single crystal, and then flexoelectric polarization occurred along a certain direction. The flexoelectric polarization field was formed at the Si single crystal with a range of lengths or volumes. This is the flexoelectronic effect operating in Si single crystals. Using the flexoelectric polarization field as a “gate” to control the current is the basis for enhancing the luminous intensity of the Si-based QLED array. The I - V characteristics with externally applied pressure are shown in Fig. 4b. Under external pressure, the current under the forward voltage increased with pressure, while the current under the reverse voltage first increased and gradually reached a maximum value in an asymmetric process. Figure 4d shows the ratio of the change in current to the initial current under the stress gradient. As the force continued to increase, there was an asymmetric change curve under forward and reverse voltages, which corresponded to the current change in devices based on Si micropillars as a function of loading pressure, as shown in Fig. 4c.

The changes in the electronic transport characteristics mainly arose from two effects: the piezoresistive effect and the flexoelectronic effect, both of which may contribute to the increase in current.

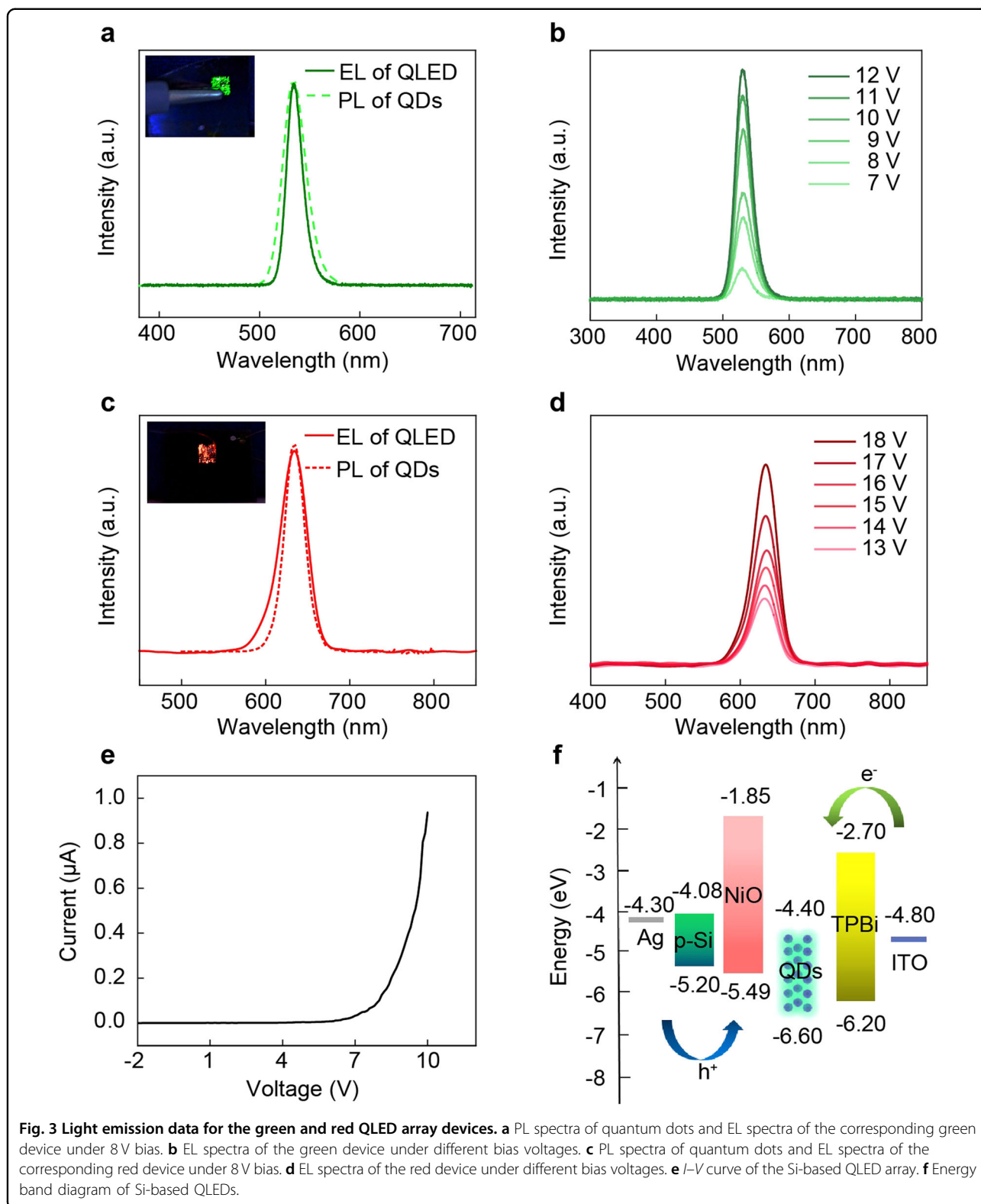
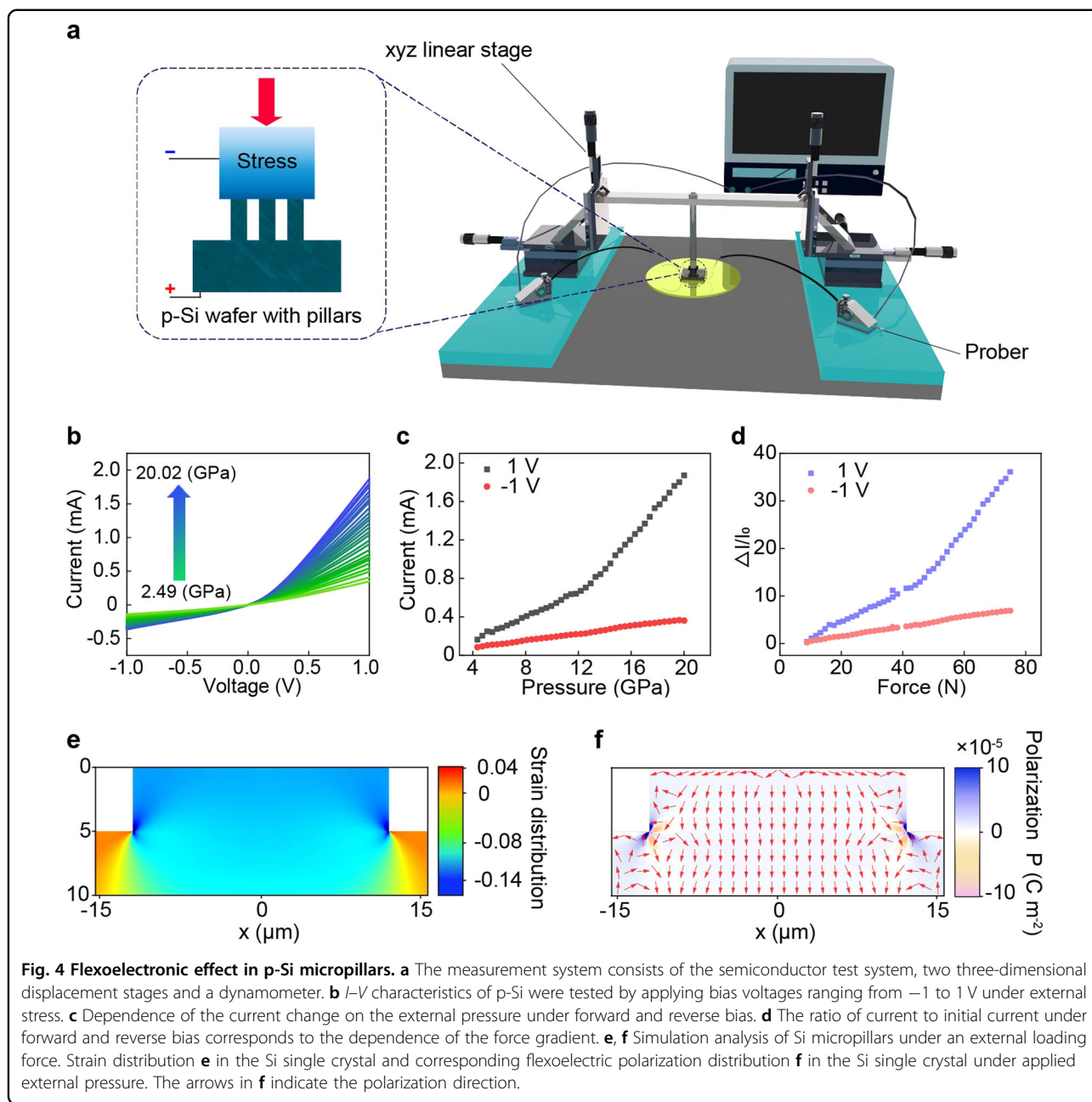


Fig. 3 Light emission data for the green and red QLED array devices. **a** PL spectra of quantum dots and EL spectra of the corresponding green device under 8 V bias. **b** EL spectra of the green device under different bias voltages. **c** PL spectra of quantum dots and EL spectra of the corresponding red device under 8 V bias. **d** EL spectra of the red device under different bias voltages. **e** I - V curve of the Si-based QLED array. **f** Energy band diagram of Si-based QLEDs.

However, the piezoresistive effect is a symmetrical volume effect without polarity, and hence, the I - V curves should show symmetrical changes under forward and

reverse voltages, which has been demonstrated and is shown in Fig. S1. In addition, the piezoresistive coefficient of Si is approximately $93.5 \times 10^{-11} \text{ Pa}^{-1}$, which is much



smaller than our experimental result (approximately $179.8 \times 10^{-11} \text{ Pa}^{-1}$ in Fig. S4). The current change caused by the piezoresistive effect was small, which indicates that there was a flexoelectronic effect. Under external pressure, the local strain gradient was generated at the bottom of the Si micropillars (Fig. 4e), which induced the flexoelectric polarization field (Fig. 4f). This will have a significant influence on the concentration and distribution of free carriers and hence on the carrier transport characteristics. Due to the polarity of flexoelectric polarization, there is an asymmetric modulation effect operating on the device current under forward and reverse bias.

Moreover, based on our results, the flexoelectronic effect may even play a major role in the regulation process. Therefore, the current increase under external pressure may be caused by a combination of the piezoresistive effect and the flexoelectronic effect.

After studying the flexoelectronic effect of a Si single crystal, a Si-based QLED array was fabricated, and the light emission intensity of the QLED was regulated with the strain coupling effect. A measurement system prepared from an inverted microscope and 3D stages was used to measure the modulation effect of strain coupling on the light emission performance of the Si-based QLED

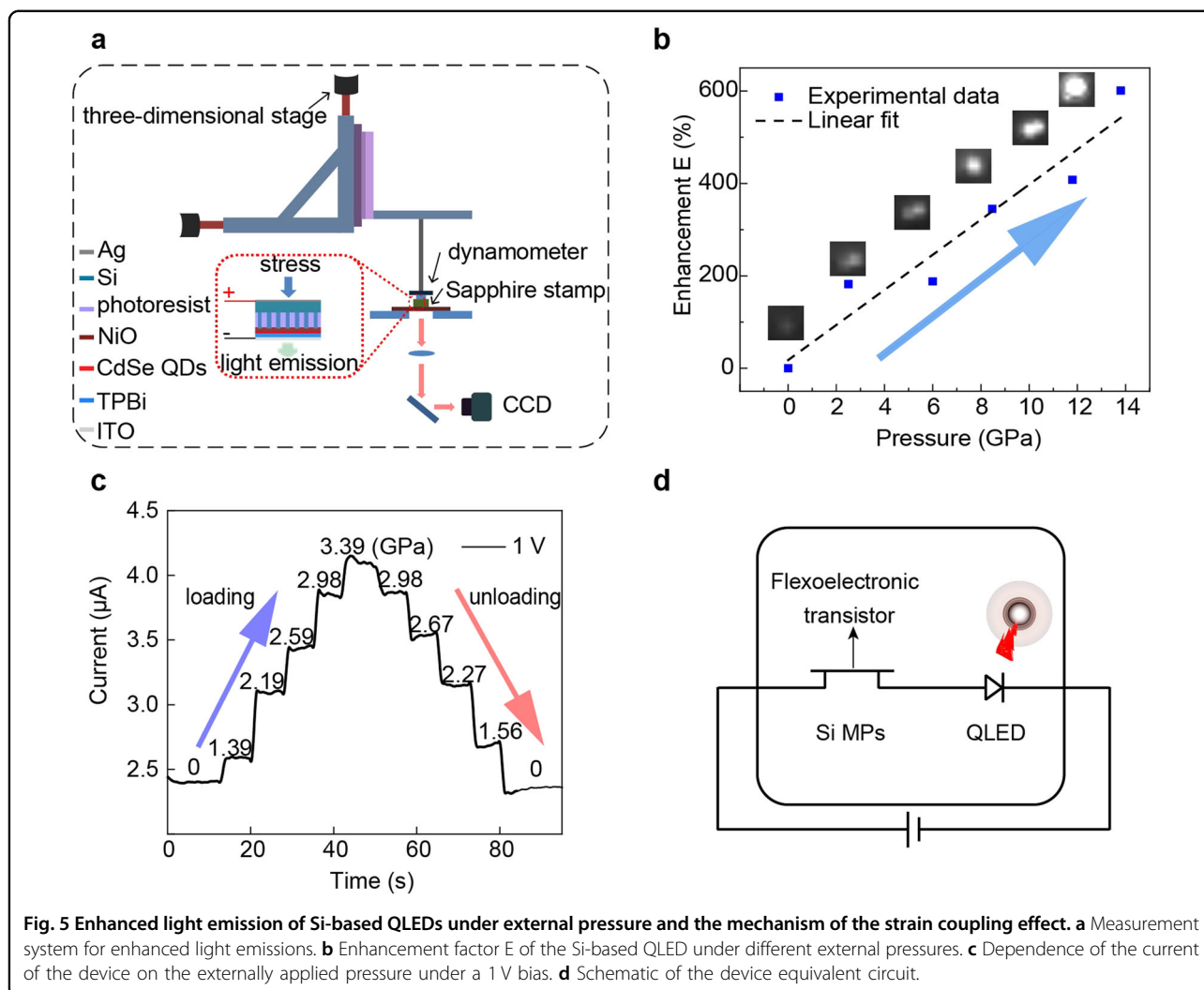


Fig. 5 Enhanced light emission of Si-based QLEDs under external pressure and the mechanism of the strain coupling effect. **a** Measurement system for enhanced light emissions. **b** Enhancement factor E of the Si-based QLED under different external pressures. **c** Dependence of the current of the device on the externally applied pressure under a 1 V bias. **d** Schematic of the device equivalent circuit.

array, as shown in Fig. 5a. As shown in Fig. 5b, a higher emission density for the Si-based QLED was obtained by applying a larger external pressure, which indicates a positive correlation. The enhancement factor E is defined as $E = (I_e - I_0) / I_0$ (where I_0 is the emission intensity of the Si-based QLED without pressure, and I_e is the emission intensity under the corresponding pressure), and E is approximately linearly dependent on the external pressure. Since the stress distribution was mainly concentrated at the bottoms of the Si micropillars (Fig. S2), the polarization distribution near the Si micropillars can be regarded as that of a transistor with variable resistivity connected in series between the QLED and bulk Si below. Upon applying external pressure, the resistance of the bulk Si below remained unchanged while the Si micropillars were subjected to the local strain gradient; this resulted in flexoelectric polarization, which has a substantial influence on the concentration and distribution of free carriers of semiconductors and the current near the

interface. The reason for the enhancement of the emission intensity of the pixels in the QLED array is the strain coupling effect, in which there may be the superposition of multiple effects, and improvement of the current by the flexoelectric polarization field will also increase the emission intensity of the pixels. Figure 5c shows that under a fixed bias voltage of 1 V, a change in device current conforms to step-by-step loading and release of the applied pressure. According to the equivalent circuit of the device shown in Fig. 5d, the Si micropillars act as a flexoelectronic transistor connected with a QLED in series and control the current in the circuit with the flexoelectric field distributions in Si micropillars under external pressure. This equivalent circuit model was proposed and discussed in our previous work¹⁹.

Conclusions

In summary, a Si-based QLED array was designed and fabricated in this paper. The p-Si was etched into a

micropillar array and directly used as a hole transport layer; hence, the size and resolution of the pixel array can be controlled by lithography and etching parameters. By introducing the mechanism for strain coupling regulation in the Si-based QLED array device, the carrier transport process can be modulated by the flexoelectronic effect in the Si single crystal, and the emission density of the Si-based QLED array device is enhanced. Under an external pressure of 13.8 GPa, the emission density of the Si-based QLED array was enhanced by 600%. Combined with the excellent optical properties of QDs, our device can achieve a narrow emission spectrum and adjustable emission wavelength, which will be a promising strategy for broadening the applications of Si-based photonic devices and showing application potential in MEMS, electronic skin, human-machine interfaces and tactile sensors.

Acknowledgements

The authors are grateful for the support of the National Natural Science Foundation of China (52192610, U20A20166, 61805015, 52125205, and 61804011), the National Key R&D Program of China (2021YFB3200302 and 2021YFB3200304), the Natural Science Foundation of Beijing Municipality (Z180011 and 2222088), the Shenzhen Science and Technology Program (Grant No. KQTD20170810105439418), and the Fundamental Research Funds for the Central Universities.

Author details

¹School of Chemistry and Chemical Engineering, Guangxi University, Nanning, Guangxi 530004, P. R. China. ²CAS Center for Excellence in Nanoscience, Beijing Key Laboratory of Micronano Energy and Sensor, Beijing Institute of Nanoenergy and Nanosystems, Chinese Academy of Sciences, Beijing 100083, P. R. China. ³Research Laboratory for Quantum Materials, Singapore University of Technology and Design, Singapore 487372, Singapore. ⁴Center on Nanoenergy Research, School of Physical Science and Technology, Guangxi University, Nanning, Guangxi 530004, P. R. China. ⁵School of Nanoscience and Technology, University of Chinese Academy of Sciences, Beijing 100049, P. R. China

Author contributions

YM and XF contributed equally to this work. YM contributed to the paper writing and data analysis. YM performed the experiments. XF contributed to the simulation analysis. LZ and RH contributed to the discussion. RB proposed and conceived the study. CP led the preparation of the manuscript with contributions from all authors.

Conflict of interest

The authors declare no competing interests.

Publisher's note

Springer Nature remains neutral with regard to jurisdictional claims in published maps and institutional affiliations.

Supplementary information The online version contains supplementary material available at <https://doi.org/10.1038/s41427-022-00430-3>.

Received: 3 June 2022 Revised: 31 July 2022 Accepted: 11 August 2022
Published online: 14 October 2022

References

- Liu, Y. et al. Biodegradable, breathable leaf vein-based tactile sensors with tunable sensitivity and sensing range. *Small* **18**, e2106906 (2022).

- Ren, J. et al. A graphene rheostat for highly durable and stretchable strain sensor. *InfoMat* **1**, 396–406 (2019).
- Tao, J. et al. Real-time pressure mapping smart insole system based on a controllable vertical pore dielectric layer. *Microsyst. Nanoeng.* **6**, 62 (2020).
- Zhao, X., Hua, Q., Yu, R., Zhang, Y. & Pan, C. Flexible, stretchable and wearable multifunctional sensor array as artificial electronic skin for static and dynamic strain mapping. *Adv. Electron. Mater.* **1**, 1500142 (2015).
- Ge, G. et al. Muscle-inspired self-healing hydrogels for strain and temperature sensor. *ACS nano* **14**, 218–228 (2020).
- Liu, H. et al. Stretchable conductive nonwoven fabrics with self-cleaning capability for tunable wearable strain sensor. *Nano Energy* **66**, 104143 (2019).
- Liu, Y. et al. Recent progress in tactile sensors and their applications in intelligent systems. *Sci. Bul.* **65**, 70–88 (2020).
- Li, J. et al. Biologically inspired stretchable, multifunctional, and 3D electronic skin by strain visualization and triboelectric pressure sensing. *Small Sci.* **2**, 2100083 (2021).
- Zhu, R. et al. Anisotropic magnetic liquid metal film for wearable wireless electromagnetic sensing and smart electromagnetic interference shielding. *Nano Energy* **92**, 106700 (2022).
- Hua, Q. et al. Bioinspired electronic whisker arrays by pencil-drawn paper for adaptive tactile sensing. *Adv. Electron. Mater.* **2**, 1600093 (2016).
- Wang, C. et al. Mechanoluminescent hybrids from a natural resource for energy-related applications. *InfoMat* **3**, 1272–1284 (2021).
- Wang, X. et al. Dynamic pressure mapping of personalized handwriting by a flexible sensor matrix based on the mechanoluminescence process. *Adv. Mater.* **27**, 2324–2331 (2015).
- Bao, R., Tao, J., Pan, C. & Wang, Z. L. Piezophototronic effect in nanosensors. *Small Sci.* **1**, 2000060 (2021).
- Wang, Z. L. Progress in piezotronics and piezo-phototronics. *Adv. Mater.* **24**, 4632–4646 (2012).
- Pan, C. et al. High-resolution electroluminescent imaging of pressure distribution using a piezoelectric nanowire LED array. *Nat. Photonics* **7**, 752–758 (2013).
- Bao, R. et al. CdS nanorods/organic hybrid LED array and the piezo-phototronic effect of the device for pressure mapping. *Nanoscale* **8**, 8078–8082 (2016).
- Liu, T. et al. Piezo-phototronic effect in InGaN/GaN semi-floating micro-disk LED arrays. *Nano Energy* **67**, 104218 (2020).
- Bao, R. et al. Flexible and controllable piezo-phototronic pressure mapping sensor matrix by ZnO NW/p-Polymer LED Array. *Adv. Funct. Mater.* **25**, 2884–2891 (2015).
- Bao, R. et al. Light-emission enhancement in a flexible and size-controllable ZnO nanowire/organic light-emitting diode array by the piezotronic effect. *ACS Photonics* **4**, 1344–1349 (2017).
- Faria, J. C. D., Campbell, A. J. & McLachlan, M. A. ZnO Nanorod arrays as electron injection layers for efficient organic light emitting diodes. *Adv. Funct. Mater.* **25**, 4657–4663 (2015).
- Peng, Y. et al. Achieving high-resolution pressure mapping via flexible GaN/ZnO nanowire LEDs array by piezo-phototronic effect. *Nano Energy* **58**, 633–640 (2019).
- Wang, C. et al. Enhanced emission intensity of vertical aligned flexible ZnO nanowire/p-polymer hybridized LED array by piezo-phototronic effect. *Nano Energy* **14**, 364–371 (2015).
- Li, X. et al. Flexible light emission diode arrays made of transferred Si microwires-ZnO nanofilm with piezo-phototronic effect enhanced lighting. *ACS nano* **11**, 3883–3889 (2017).
- Liu, H. et al. Lightweight, superelastic, and hydrophobic polyimide nanofiber/MXene composite aerogel for wearable piezoresistive sensor and oil/water separation applications. *Adv. Funct. Mater.* **31**, 2008006 (2021).
- Han, X. et al. Recent progress in optoelectronic synapses for artificial visual-perception system. *Small Struct.* **1**, 2000029 (2020).
- Huo, Z. et al. High-performance Sb-doped p-ZnO NW films for self-powered piezoelectric strain sensors. *Nano Energy* **73**, 104744 (2020).
- Pan, C. et al. Progress in piezo-phototronic-effect-enhanced light-emitting diodes and pressure imaging. *Adv. Mater.* **28**, 1535–1552 (2016).
- Qiao, S. et al. ZnO nanowire based CIGS solar cell and its efficiency enhancement by the piezo-phototronic effect. *Nano Energy* **49**, 508–514 (2018).

29. Sun, J. et al. MXene enhanced self-powered alternating current electroluminescence devices for patterned flexible displays. *Nano Energy* **86**, 106077 (2021).
30. Wen, X. et al. Development and progress in piezotronics. *Nano Energy* **14**, 276–295 (2015).
31. Yang, Z. et al. A high performance CsPbBr₃ microwire based photodetector boosted by coupling plasmonic and piezo-phototronic effects. *Nano Energy* **85**, 105951 (2021).
32. Zhou, R., Hu, G., Yu, R., Pan, C. & Wang, Z. L. Piezotronic effect enhanced detection of flammable/toxic gases by ZnO micro/nanowire sensors. *Nano Energy* **12**, 588–596 (2015).
33. Zhang, M. et al. Ultrasoft quantum dot micropatterns by a facile controllable liquid-transfer approach: low-cost fabrication of high-performance QLED. *J. Am. Chem. Soc.* **140**, 8690–8695 (2018).
34. Abbamonte, P. et al. Crystallization of charge holes in the spin ladder of Sr₁₄Cu₂₄O₄₁. *Nature* **431**, 1078–1081 (2004).
35. Li, X. et al. Enhancing light emission of ZnO-nanofilm/Si-micropillar heterostructure arrays by piezo-phototronic effect. *Adv. Mater.* **27**, 4447–4453 (2015).
36. Chen, M. et al. Tuning light emission of a pressure-sensitive Si/ZnO nanowires heterostructure matrix through piezo-phototronic effects. *ACS nano* **10**, 6074–6079 (2016).
37. Bhaskar, U. K. et al. A flexoelectric microelectromechanical system on Si. *Nat. Nanotechnol.* **11**, 263–266 (2016).
38. Zubko, P., Catalan, G. & Tagantsev, A. K. Flexoelectric effect in solids. *Annu. Rev. Mater. Res.* **43**, 387–421 (2013).
39. Cross, L. E. Flexoelectric effects: charge separation in insulating solids subjected to elastic strain gradients. *J. Mater. Sci.* **41**, 53–63 (2006).
40. Das, S. et al. Enhanced flexoelectricity at reduced dimensions revealed by mechanically tunable quantum tunnelling. *Nat. Commun.* **10**, 537 (2019).
41. Wu, M. et al. Flexoelectric thin-film photodetectors. *Nano Lett.* **21**, 2946–2952 (2021).
42. Wang, L. et al. Flexoelectronics of centrosymmetric semiconductors. *Nat. Nanotechnol.* **15**, 661–667 (2020).
43. Hong, J. & Vanderbilt, D. First-principles theory and calculation of flexoelectricity. *Phys. Rev. B* **88**, 174107 (2013).